

Simulation of Atomic Cadmium Spectroscopy in Rare Gas Solids Using Pair Potentials[†]

Brendan Healy and John G. McCaffrey*

Department of Chemistry, National University of Ireland, Maynooth, County Kildare, Ireland

Received: October 5, 1999; In Final Form: November 17, 1999

Luminescence in the vacuum UV/visible region has been recently recorded for atomic cadmium isolated in the rare gas solids Ne, Ar, Kr, and Xe, and because of the availability of diatomic Cd·RG and RG·RG pair potentials, theoretical calculations are now performed and compared to the recorded luminescence spectra. Calculations were first done for the gas-phase excited-state cluster species Cd(¹P₁)·RG_{*n*}, where *n* is the number of rare gas atoms in the cluster. The Cd·RG₄, Cd·RG₅, and Cd·RG₆ clusters showed energy minima for the Cd p_z orbital situated at the center of the planar rare gas clusters. With the rare gas distances in the planar clusters fixed at the rare gas dimer bond lengths, the cluster showing the greatest stabilization was the Cd·RG₅ species. The cluster calculations were then extended into the solid state for Cd occupying a single substitutional site of the solid rare gas lattice. Two vibronic modes lead to a preferential interaction between the guest and four rare gas atoms, thereby reducing the excited-state energy and leading to distinct minima. The modes are (a) the “body” mode (Q₂), which involves the motion of the Cd atom toward an octahedral interstitial site and (b) the “waist” mode (Q₃), which involves the in-phase contraction of four rare gas atoms in a single plane toward the Cd atom. Calculations based on single substitutional site occupancy of Cd in the rare gases indicate excited state stabilization for the waist mode for all hosts except neon. The body mode exhibits stabilization in Kr and Xe only. The pair of singlet emission bands observed in the Cd/Kr system is identified as originating from the stabilization of both vibronic modes in the excited state. The lack of stabilization for either mode in Ne, even though singlet emission exists in Cd/Ne, is indicative that a multivacancy site occupancy is likely here.

Introduction

Much experimental work has been done on the luminescence of (*ns*)² metal atoms isolated in rare gas solids, e.g., Mg,¹ Zn,² Hg,³ and Cd,⁴ and with the increasing amount of spectroscopic data becoming available for diatomic metal atom/rare gas atom van der Waals molecules, it is now possible to predict absorption and emission wavelengths. The cadmium spectroscopy results analyzed here involves the 5s²–5s¹5p¹ transition, which is similar to the Zn 4s²–4s¹4p¹ system for which previous work on both experimental and predicted luminescence already exists.^{2,5} From calculations done on the excited-state Zn(¹P₁)/RG (RG = Ar, Kr, and Xe) matrix systems, it was shown that interactions between the excited-state guest Zn atom and four host rare gas atoms achieved the energy minima in the solid state. Two vibronic modes lead to such interactions and thereby to distinct energy minima. One mode involves motion of the guest atom from the substitutional site into an adjacent octahedral site, the other contraction of four lattice atoms toward the guest atom. This localized pair potential approach was used successfully to identify the origin of pairs of emission bands in the Zn/Ar, Zn/Kr, and Zn/Xe systems as being due to the existence of two energy-lowering vibronic modes in the excited ¹T_{1u} state. The pair potential method is now applied to matrix-isolated atomic cadmium where size effects, arising from this larger guest atom occupying the fixed site sizes in the solid rare gases, should be identifiable.

A summary of the luminescence recorded for the Cd/RG solids is shown in Figure 1. Optical measurements were

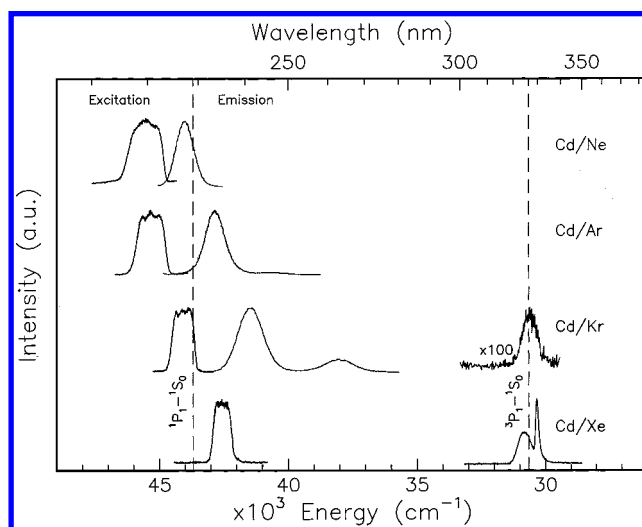


Figure 1. Excitation and emission profiles recorded at 4 K for annealed Cd/RG samples. For comparison, the 5s¹5p¹ ¹P₁ ↔ 5s² ¹S₀ and 5s¹5p¹ ³P₁ ↔ 5s² ¹S₀ gas-phase transitions of atomic cadmium are included. All features have been normalized for clarity. An indication of the weakness of the Cd/Kr triplet emission compared with the singlet emission band at 241.5 nm is given by the indicated gain.

conducted at the HIGITI experimental station in HASYLAB at DESY, Hamburg, utilizing synchrotron radiation. The experimental setup has been presented in detail before.⁴ Solid Cd/RG samples were prepared by the cocondensation of cadmium metal vapor, produced by electron bombardment of 1 mm thick cadmium foil coiled in a molybdenum crucible in an Omicron EFM3 UHV evaporator, with the rare gases. As shown in Figure

[†] Part of the special issue “Marilyn Jacox Festschrift”.

* To whom correspondence should be addressed.

1, both Cd/Ne and Cd/Ar have one emission band assigned, from lifetime measurements,⁴ to the singlet $5s^1 5p^1 \ ^1P_1 \rightarrow 5s^2 \ ^1S_0$ transition. In Cd/Kr, as in the Zn/Ar and Zn/Kr systems,² a pair of emission bands is observed, both of which are assigned to the singlet transition. Sample annealing⁴ showed that the pair of Cd/Kr bands arise from a single thermally stable site. The absorption features of the Cd/Ar, Cd/Kr, and Cd/Xe systems show a 3-fold splitting pattern⁴ that is not evident in the Cd/Ne absorption feature.^{4,6} Cd/Xe has two long-lived emission bands in the near-UV region that, based on their spectral locations, are assigned to $5s^1 5p^1 \ ^3P_1 \rightarrow 5s^2 \ ^1S_0$ transitions. Because of their long decay times, only tentative *J* value assignments have been made because of the lack of precise lifetimes⁴ when measurement attempts were made using high repetition synchrotron radiation for excitation.

The task of the present work is to simulate the Cd/RG matrix emission using a localized pair potentials approach. Its objective is an examination of the approach, applied with success in the Zn/RG matrix systems, to identify the effect of this larger guest in the well-defined site sizes of the solid rare gases. The paper is organized as follows. First, gas-phase type calculations are done for atomic Cd interacting with rare gas cluster systems. These calculations provide an insight into the interactions occurring in the solid state, which are then calculated.

Method

A localized approach is adopted to simulate the energies of the solid-state Cd/RG systems involving pairwise-summing of the interactions between the guest Cd atom and a limited number of host atoms. The method employed is that developed by Beswick and co-workers^{7,8} in a simulation of the vibronic structure of the gas-phase triatomic $\text{Hg}(^3P_1)\cdot\text{Ar}_2$ complex. Crepin and Tramer³ made initial attempts at applying this method to the $\text{Hg}(^3P_1)/\text{RG}$ matrix systems. More recently, calculations on the solid-state $\text{Zn}(^1P_1)/\text{RG}$ systems were performed by McCaffrey and Kerins^{5,9} to explain the origin of the observed pairs of matrix emission bands.

The two key assumptions in the method are (1) that the energy of the multibody system, cluster, or solid state is calculated from the sum of metal atom–rare gas atom interactions and (2) that the interactions in the solid state are short range. In Table 1 the Cd•RG pair-potential parameters used for the Cd/RG matrix simulations are presented. These parameters have been obtained from the work of Breckenridge and co-workers.^{10,11} Laser-induced fluorescence spectroscopy was used in the derivation of parameters needed for the bound ground $X^1\Sigma_0$ and excited $C^1\Pi_1$ and $D^1\Sigma$ states of the Cd•RG diatomics. In Figure 2, the Cd•Kr potential energy curves and their associated orbital interactions in the ground $X^1\Sigma_0$ and excited $D^1\Sigma$ and $C^1\Pi_1$ states are depicted. Both the ground $X^1\Sigma_0$ and excited $D^1\Sigma$ state curves were originally represented by the Buckingham functions,¹² of the form $A e^{-bR} - C_6/R^6$, listed in Table 2. In the present work, the original $D^1\Sigma$ curve is fit to a Morse function in order to remove the nonphysical behavior in the Buckingham potential energy function, evident in the right panel of Figure 3, below 3.3 Å. The ground-state RG•RG parameters used were the values listed by Kaup and Breckenridge.¹³

Calculations and Results

Only an outline of the calculations will be given here because they have already been described elsewhere⁵ in detail. In the ground electronic state, the cluster potential $W_X(R)$ is given by

TABLE 1: Morse $D_e[1 - e^{-\beta(R-R_e)}]^2$ and Repulsive Exponential ($A e^{-bR}$) Function Parameters Used as Bound and Free State Pair Potentials, Respectively, for Atomic Rare Gas–Rare Gas and Cadmium–Rare Gas Atom Interactions^a

diatomic	D_e (cm ⁻¹)	R_e (Å)	β (Å ⁻¹)	A ($\times 10^7$ cm ⁻¹)	b (Å ⁻¹)
Ne•Ne ($X^1\Sigma$)	29.413	3.090	2.839		
Ar•Ar ($X^1\Sigma$)	99.2	3.761	1.685		
Kr•Kr ($X^1\Sigma$)	138.4	4.017	1.604		
Xe•Xe ($X^1\Sigma$)	196.24	4.3634	1.509		
Cd•Ne ($X^1\Sigma$)	39	4.26	1.0785		
Cd•Ar ($X^1\Sigma$)	106	4.31	1.212		
Cd•Kr ($X^1\Sigma$)	128	4.33	1.28		
Cd•Xe ($X^1\Sigma$)	187	4.55	0.9917		
Cd•Ne ($C^1\Pi$)	89	3.61	1.350		
Cd•Ar ($C^1\Pi$)	544	3.28	1.399		
Cd•Kr ($C^1\Pi$)	1036	3.17	1.5236		
Cd•Xe ($C^1\Pi$)	2485	3.26	1.6686		
Cd•Ne ($D^1\Sigma$)				1.537791 ^d	2.9408 ^d
Cd•Ar ($D^1\Sigma$)				0.068136 ^b	1.7775 ^b
Cd•Kr ($D^1\Sigma$)	79.51 ^c	5.977 ^c	0.715 ^c		
Cd•Xe ($D^1\Sigma$)				1.5856 ^d	2.35627 ^d

^a The Cd•RG parameters were obtained from refs 10 and 11 and the RG•RG data from ref 12. ^b Repulsive exponential function fitted to $A e^{-bR} - C_6/R^6$ potential energy curve. ^c Morse function fitted to $A e^{-bR} - C_6/R^6$ potential energy curve. ^d Estimated fits of plots in refs 10 and 11.

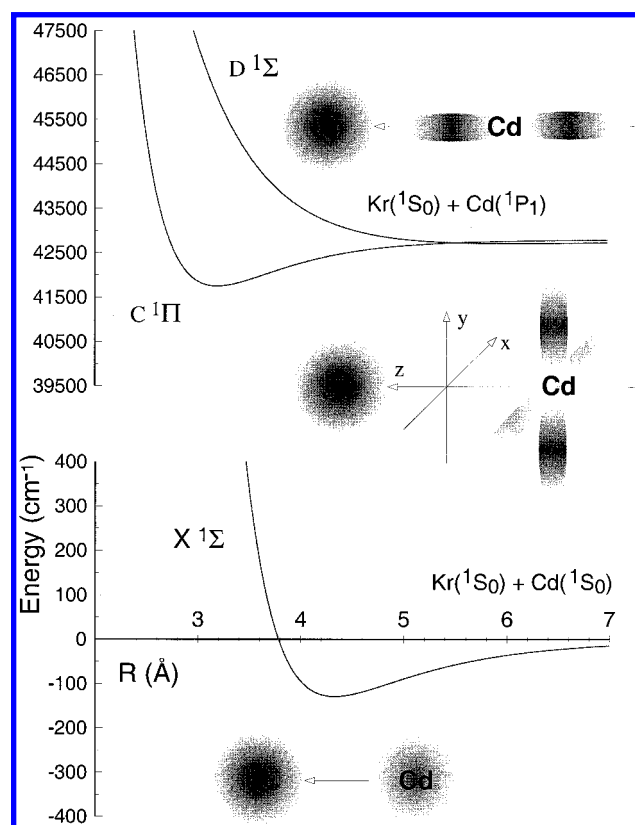


Figure 2. Potential energy curves of the diatomic van der Waals molecule Cd•Kr induced by the interaction of the Cd 1S_0 ground and 1P_1 excited state with the krypton 1S_0 state.

where k is the number and R_k the length of the cadmium atom–rare gas atom bonds in the cluster and m represents the number of rare gas–rare gas interactions involved in the Cd•RG_{*n*} cluster. Since transition energies are being calculated in the spectral simulations, the $V_{\text{RG-RG}}$ term will only be stated explicitly in the expressions following when a change in the RG–RG bond length occurs. Formulas of the first excited electronic state Cd•(1P_1)•RG_{*n*} are more difficult to obtain than that of the ground state because of the nonzero electronic angular momentum

TABLE 2: Original Parameters for the Cd·Kr D¹Σ Excited State from Ref 10^a

D ¹ Σ State				
	range (Å)	A (cm ⁻¹)	b (Å ⁻¹)	C ₆ (cm ⁻¹ Å ⁶)
Cd·Ar	3.7–5.0	-4.5979	-0.6758	-2.5767 × 10 ⁶
Cd·Kr	3.8–5.0	1.4731 × 10 ⁶	1.5399	1.0396 × 10 ⁷
X ¹ Σ State				
	A (cm ⁻¹)	b (Å ⁻¹)	C ₆ (cm ⁻¹ Å ⁶)	
Cd·Ar	1.116 × 10 ⁷	2.6618	1.4244 × 10 ⁶	
Cd·Kr	1.7026 × 10 ⁷	2.712	1.7433 × 10 ⁶	

^a The ranges given for the D¹Σ state are used to fit the model potential to the experimental data.

$$W_X(R) = \sum_{k=1}^n V_{\text{Cd}\cdot\text{RG}}(R_k) + \sum_{j=1}^m V_{\text{RG}\cdot\text{RG}}(r_j) \quad (1)$$

(EAM) of the ¹P₁ level. The formulas are obtained by projecting the EAM of the diatomic Cd–RG axis onto the cluster axis using Wigner rotation matrices.¹⁴ Because of the axial symmetry of the Cd(¹P₁) state, the following three cluster potentials, $W_n(R)$,

$$p_z: W_1(R) = \sum_{k=1}^n \cos^2 \theta_k V_{\Sigma}(R_k) + \sin^2 \theta_k V_{\Pi}(R_k) \quad (2)$$

p_x :

$$W_2(R) = \sum_{k=1}^n \sin^2 \theta_k \cos^2 \phi_k V_{\Sigma}(R_k) + [\cos^2 \theta_k \cos^2 \phi_k + \sin^2 \phi_k] V_{\Pi}(R_k) \quad (3)$$

p_y :

$$W_3(R) = \sum_{k=1}^n \sin^2 \theta_k \sin^2 \phi_k V_{\Sigma}(R_k) + [\cos^2 \theta_k \sin^2 \phi_k + \cos^2 \phi_k] V_{\Pi}(R_k) \quad (4)$$

arise for the three atomic p orbitals. In eqs 2–4, the C¹Π₁ and D¹Σ state potentials of the Cd·RG diatomics are represented as V_{Π} and V_{Σ} , respectively. The meanings of the variables θ and ϕ are illustrated in Figure 4, which shows a Cd p_z orbital approaching perpendicular to a plane containing four rare gas atoms arranged in a square. θ_k are the angles between the approach axis of the Cd p_z orbital and the rare gas atoms in the cluster species, ϕ_k are the angles between the rare gas atoms in the square plane. R_{CM} is the distance of the Cd atom to the center-of-mass of the rare gas cluster. Thus, in the treatment used, direct pairwise addition of the potentials is only done for the ground state with eq 1. In the excited state, the angular dependence is accounted for in eqs 2–4 prior to addition of the potentials.

Clusters. Calculations were performed on the Cd·RG_{*n*} clusters, with $n = 3, 4, 5$, or 6. The Cd atom is permitted to approach perpendicular to the planar arrangement of rare gas atoms as shown in Figure 4. The cluster potential energies for the C_{4v} , $n = 4$ case were obtained by substituting the values $\pi/2$, π , $3\pi/2$, and 2π for ϕ_k into eqs 2–4. The following expressions were derived upon evaluation of the sums

$$W_{A_1}(R) = 4[\cos^2 \theta V_{\Sigma}(R) + \sin^2 \theta V_{\Pi}(R)] \quad (5)$$

$$W_E(R) = 2[\sin^2 \theta V_{\Sigma}(R) + (\cos^2 \theta + 1) V_{\Pi}(R)] \quad (6)$$

where Cd(p_z)·RG_{*n*} and Cd(p_x, p_y)·RG_{*n*} interactions are now represented by the ¹A₁ and doubly degenerate ¹E electronic states, respectively. In the high-symmetry C_{4v} cluster, a single R replaces R_k , R being defined as

$$\sqrt{R_{\text{CM}}^2 + (r_e/\sqrt{2})^2}$$

where r_e is the rare gas dimer bond length in the cluster.

In Figure 5, the ¹A₁ state potential curves are shown for the approach of the p_z orbital to the planar Kr_{*n*} clusters, $n = 3, 4, 5$, or 6. For $n = 3$ no stability was obtained, but for the other clusters maximum stabilization is attained at $R_{\text{CM}} = 0$, where the Cd p_z orbital is located at the center of the planar rare gas arrangements. It is evident in Figure 5 that the Cd(¹P₁)·RG₅ cluster is the most stable system, as demonstrated by its large binding energy of 4670.3 cm⁻¹. These results were also obtained for the other rare gas systems analyzed, with the exception of neon where the Cd(¹P₁)·Ne₆ cluster was the only one showing stabilization. Calculations of the ¹E states, although not shown, indicated energy increases; i.e., the interactions become repulsive as the Cd(p_x, p_y) orbitals approach the centers of the rare gas clusters. Thus, in the analysis of the luminescence in these cluster species, only the ¹A₁ state will be considered¹⁵ because of it being the only one to bring about a lowering of the excited-state energy.

Calculations were also done to obtain the potential energy of an excited ¹P₁ state Cd atom advancing in a C_{4v} approach toward the base of a square pyramidal RG₅ cluster. The result of this cluster calculation is of importance to the solid state because it corresponds to the motion of a guest atom into an octahedral interstitial site of the lattice. In this C_{4v} calculation, the four rare gas atoms making up the base of the square pyramid are arranged perpendicular to the Cd atom, and the fifth apex atom is positioned on the approach axis. As the Cd p_z orbital moves toward the center of this base, it will experience repulsion from the apical rare gas atom. Thus, when the energy of the ¹A₁ state is evaluated, the repulsive term $V_{\Sigma}(R+r)$ must be added to eq 5, where r is the distance from the center of the base of the square pyramid to the apex. Equation 6, allowing calculation of the ¹E state, will have an attractive $V_{\Pi}(R+r)$ term included for the p_x, p_y approach. In Figure 6, the energy calculations of the ¹A₁ and ¹E states are shown for the Cd·Kr₅ system in a C_{4v} approach. It is readily seen that the energy minimum is not at $R = 0$, observed for the planar Cd·Kr_{*n*} cluster calculations but is at a distance 1.04 Å from the base of the Kr square pyramid. The reason for the difference originates from the apical Kr atom in the Kr₅ structure, which does not allow the Cd p_z orbital to reach the base of the pyramid, as repulsive forces are induced between the two atoms along this axis.

The Cd(¹P₁)·RG_{*n*} cluster results can now be extended into the solid-state calculations because they give us an idea of the excited-state stabilization arising from motion of the atomic guest in the solid rare gas lattices.

Matrix. The solid rare gases have a face-centered cubic (fcc) packing structure. From a comparison of the Cd·RG X¹Σ₀ ground-state bond lengths with the site sizes listed in Table 3 for the solid rare gases, it is evident that the substitutional site provides the best match for most of the rare gases. Thus, the initial calculations were done by allowing the Cd atom to replace a single rare gas atom in the rare gas lattice. This substitutional site has cubooctahedral symmetry. Therefore, (1) equivalent interactions exist for p_x, p_y , and p_z orbital occupancy and (2) ¹A_{1g} and ¹T_{1u} state labels replace the ¹S₀ and ¹P₁ designations, respectively.

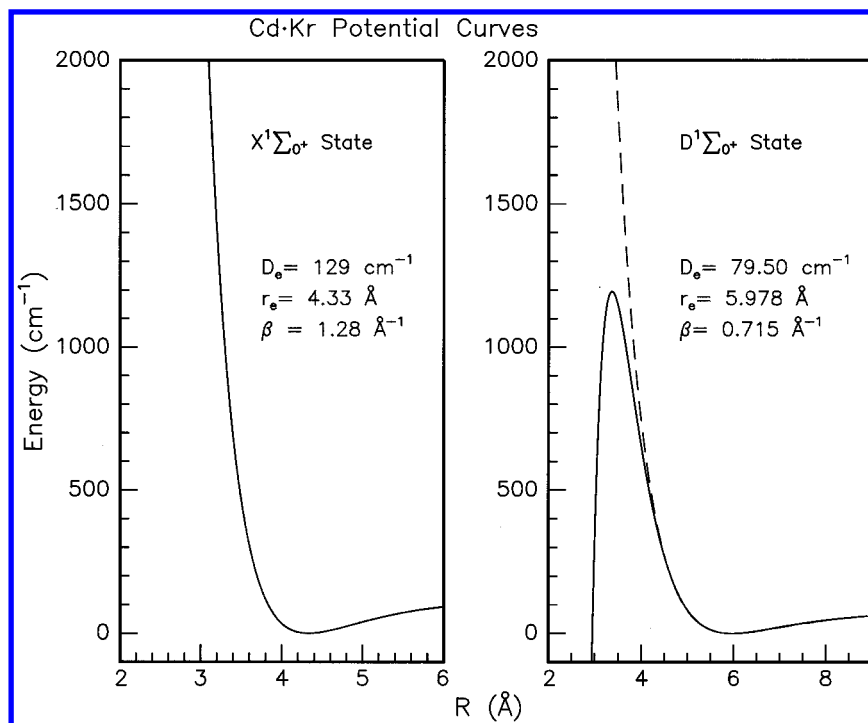


Figure 3. Fit of a Morse function $D_0[1 - e^{-\beta(R-R_e)}]^2$ to the Cd·Kr $X^1\Sigma_0$ and $D^1\Sigma$ potential energy curves represented by the function $Ae^{-bR} - C_6/R^6$ of ref 10. As can be seen in the right panel, the original $D^1\Sigma$ potential energy curve, indicated by the solid line, exhibits nonphysical behavior below 3.3 Å. The fit, shown by the broken line, was applied to the range 4.9–9.0 Å. For the ground state, a Morse fit to the Buckingham function is identical to the original.

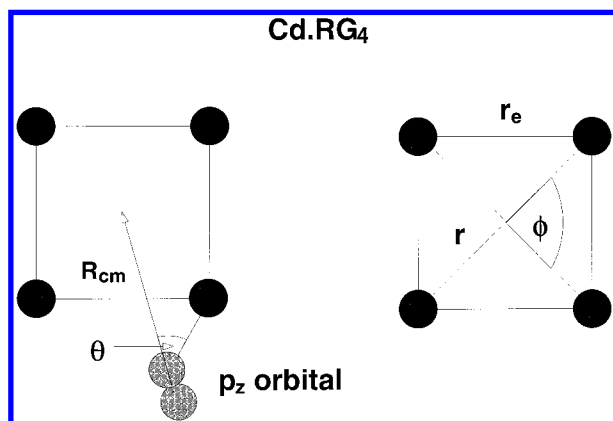


Figure 4. Diagram of the cadmium p_z orbital approaching a cluster of four rare gas atoms, i.e., $\text{Cd}(\text{P}_1)\cdot\text{RG}_4$. The angles θ and ϕ , which are specified in eqs 2–4, are shown along with the distance variables r and r_e , which are defined as the distance of each rare gas atom to the cluster center-of-mass and the rare gas–rare gas bond length, respectively.

Besides the dominant interaction of the Cd atom with the 12 nearest rare gas neighbors, the interaction of the Cd atom with the six next-nearest neighbors is needed in order to provide the required p orbital equivalency. Thus, the 18 Cd–RG interactions depicted in Figure 7 are considered. The labels $I_{\text{oh}1}$ and $I_{\text{oh}2}$ in Figure 7 denote the octahedral interstitial sites and will be important when looking at the atomic motion in the excited state.

According to the $\text{Cd}\cdot\text{Kr}_n$ cluster calculations shown in Figure 5, the interaction one should look for in the solid state to attain the greatest excited-state stabilization is the Cd(p_z) atom located at the center of a planar arrangement of five nearest-neighbor krypton atoms. However, in view of the 4-fold symmetry in the fcc lattice, this is not possible because planar arrangements of only four and six Kr atoms are possible for the 12 nearest-neighbor atoms surrounding the Cd guest in a substitutional site. Instead, we look at the dominant interaction between the Cd

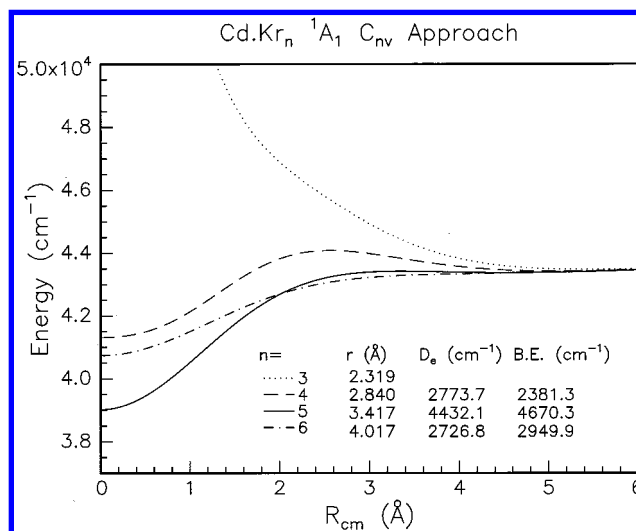


Figure 5. Potential energy plotted against the distance associated with the perpendicular approach of the cadmium p_z orbital toward the center-of-mass of the planar rare gas clusters $\text{Cd}\cdot\text{Kr}_n$, $n = 3, 4, 5,$ or 6 . The greatest stability is attained for $n = 5$, but the $n = 4$ system is of more significance to the matrix system because of the 4-fold symmetry of the solid rare gases. Also the $\text{C}^1\Pi_1$ bond length is 3.17 Å, but the Kr_4 square-planar cluster has an r value (see Figure 4) of 2.84 Å, which shows there is only a slight degree of “crampness” in the $\text{Cd}\cdot\text{Kr}_4$ system.

atom and four of its nearest neighbors as was done for the Zn/RG calculations.⁵ Figure 8 allows a visual representation of two possible motions involving a dominant interaction of the Cd atom with four Kr atoms. It will be shown later that both of these motions lower the energy in the degenerate $^1T_{1u}$ excited state. The first motion considered is the movement of the Cd atom along the Z axis of Figure 8 toward an octahedral interstitial site. This is called the “body” mode and is denoted by Q_2 . The other mode, labeled the “waist” mode (Q_3), involves

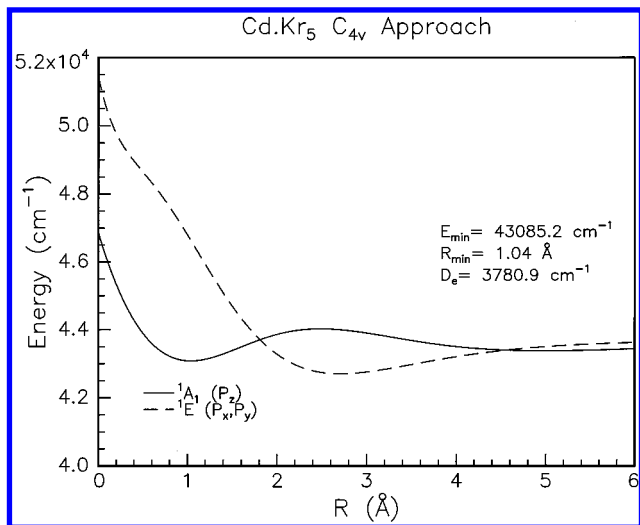


Figure 6. 1A_1 and doubly degenerate 1E potential energy curves calculated for the C_{4v} Cd·Kr₅ cluster utilizing expanded versions of eqs 5 and 6. To extend eq 5, a $V_{\Sigma}(R+r)$ is included because the Cd p_z orbital experiences repulsion from the apical Kr atom. For eq 6 a $V_{\Pi}(R+r)$ term is required to form the correct expression for the Cd p_x, p_y interaction.

TABLE 3: Comparison of the Cd-RG Internuclear Distances, r_e , in Both the Ground ($X^1\Sigma_0$) and Excited ($C^1\Pi_1$) States with the Site Diameters of the Solid Rare Gases^a

RG	a	$I_{oh,site}$	Sub. site	$r_e, X^1\Sigma_0$	$r_e, C^1\Pi_1$
Ne	4.46	1.306	3.154	4.26	3.61
Ar	5.31	1.556	3.756	4.31	3.28
Kr	5.64	1.653	3.991	4.33	3.17
Xe	6.13	1.796	4.335	4.55	3.36

^a All distances are in angstrom units, and the solid-state lattice parameters pertain to the values at 4 K.

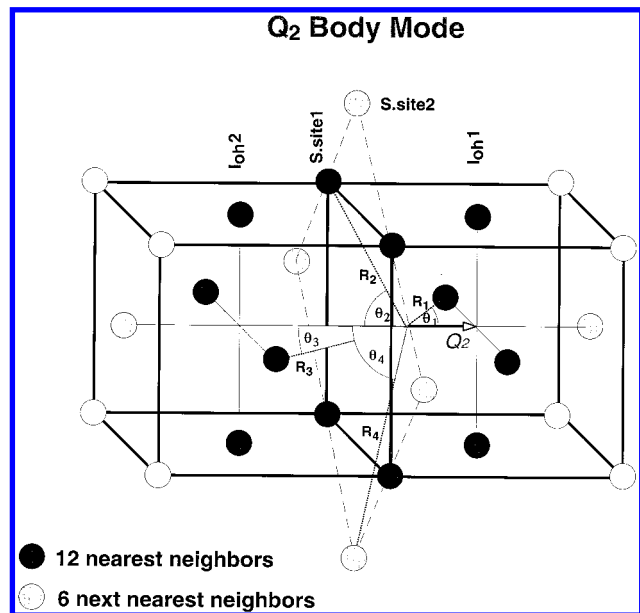


Figure 7. Diagram of a pair of adjacent fcc unit cells depicting the parameters associated with the “body mode” calculation for Cd/Kr. The Cd atom moves from S.site1 along the Z axis toward I_{oh1} denoted by Q_2 . The 12 nearest neighbors and 6 next-nearest neighbors have been shown because these atoms create the $p_x, p_y,$ and p_z equivalency in interaction terms as the Cd atom resides in a substitutional site.

four Kr atoms in the lattice XY plane contracting in-phase toward the Cd atom.

(i) *Body Mode.* As the Cd atom moves from the substitutional site toward an adjacent octahedral interstitial site I_{oh1} (see Figure

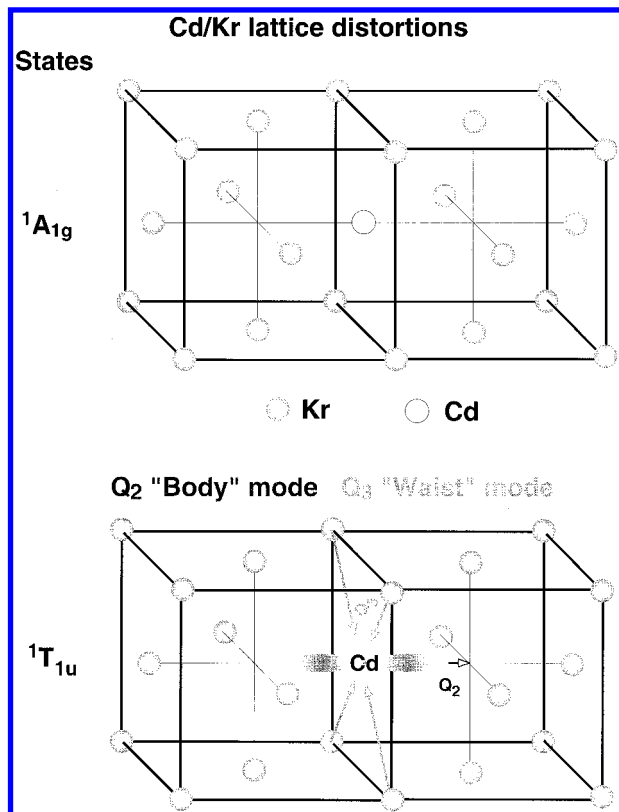


Figure 8. “Body (Q_2)” and “waist (Q_3)” mode motions within the pair of unit cells. The body mode involves the Cd(p_z) atom moving along the Z axis from the substitutional site it originally occupies in the ground state to an adjacent octahedral interstitial site. The waist mode consists of four rare gas atoms contracting in-phase toward the Cd atom.

7), four interactions must be taken into account in order to calculate the energy change arising from this motion. The four interactions all have 4-fold symmetry and are made up of the C_{4v} Cd(1P_1)·RG₄ and Cd(1P_1)·RG₅ cluster calculations presented earlier. The Cd atom moves away from I_{oh2} but gets closer to I_{oh1} and also moves away from S.site1 and S.site2 (movement toward either I_{oh1} or I_{oh2} will yield the same potential energy).

The general 1A_1 state energy expression, $W(R_n, \theta_n)$, can be derived from eq 5 for this vibronic mode and will now depend on the variables R_n and θ_n ,

$$W(R_n, \theta_n) = 4[\cos^2 \theta_n V_{\Sigma}(R_n) + \sin^2 \theta_n V_{\Pi}(R_n)] \quad (7)$$

From here we can obtain the expressions for the four interactions:

$$\begin{aligned} W(R_1, \theta_1) + V_{\Sigma}(a-q): & I_{oh1} \\ W(R_2, \theta_2): & S.site1 \\ W(R_3, \theta_3) + V_{\Sigma}(a+q): & I_{oh2} \\ W(R_4, \theta_4): & S.site2 \end{aligned} \quad (8)$$

The variable q is the linear displacement of the Cd p_z orbital away from S.site1, and a is the lattice parameter of the solid rare gas unit cell. The energies of these four interactions and their sum in a “fixed” or rigid lattice is shown for the CdKr₁₈ system in Figure 9. The Cd(p_z) energy is calculated as the atom is displaced from the center of the substitutional site ($R = 0$) where it resided in the ground state. Maximum stabilization is achieved when the Cd atom has moved 1.49 Å out of the substitutional site along the lattice Z axis. The stabilization

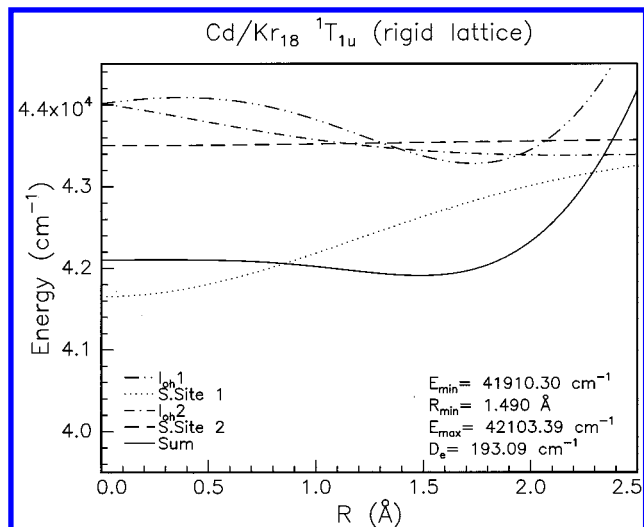


Figure 9. ${}^1T_{1u}$ excited-state energy calculation of the Cd/Kr body mode interaction. The energy is monitored as the Cd atom moves away from the substitutional site it occupies in the ground state. The four individual interactions are shown, and their sum is evaluated, which is the interaction of Cd with the 18 nearest neighbors.

energy at this displacement of 1.49 Å is 193.09 cm^{-1} as shown in Figure 9. In the Kr lattice, the distance from the center of a substitutional site to an adjacent octahedral interstitial site is 2.82 Å, so at this energy minimum the Cd (p_z) atom is positioned at a distance 1.33 Å away from the center of the nearest octahedral interstitial site.

It should be possible for the ${}^1T_{1u}$ electronic state to achieve a further lowering of its energy if the Cd atom is able to get closer to the center of the octahedral interstitial site, since there it will get nearer to achieving a complexation number of 4. However, as the Cd atom approaches along the Z axis to the center of these four Kr atoms, it will experience repulsion from the Kr atom lying on the end face, as shown in Figure 7. This Kr atom belongs to the previously described set of six next-nearest neighbor atoms. The energy of the excited state can be lowered if this end Kr atom moves into its adjacent Kr cell. This induces a destabilization within the Kr cell, but the Cd(p_z) atom will be stabilized because it can now get closer to the octahedral interstitial site. When both the stabilization and destabilization forces are equal, the excited-state minimum energy is achieved. Calculations of the Kr movement are done by looking at a Kr•Kr₁₇ system and substituting the appropriate Kr–Kr ground-state diatomic rare gas parameters from Table 1 into eq 1. The Kr atom moves 1.06 Å into the next cell, inducing a destabilization energy of 882.7 cm^{-1} in the Kr lattice. The energy calculation of the Cd(p_z) atom displacement is shown in Figure 10 and is called a relaxed lattice calculation. At the energy minimum the Cd(p_z) atom has now moved 2.09 Å away from the substitutional site originally occupied, producing a stabilization energy of 1098.6 cm^{-1} . This is over 5 times bigger than the stabilization energy for the rigid lattice calculation. At the energy minimum, the Cd(p_z) atom is situated 0.73 Å away from the octahedral interstitial site. Thus, on only moving 0.6 Å further on, going from the rigid lattice calculation to its relaxed counterpart, a 5-fold increase in the stabilization energy is achieved.

These calculations were extended to the Ne, Ar, and Xe systems using the Cd•RG potentials listed in Table 1. Figure 11 shows a summary of their relaxed lattice calculations as well as including the Cd/Kr case previously shown in Figure 10. Ground-state energies, denoted by the E'' values, are also shown

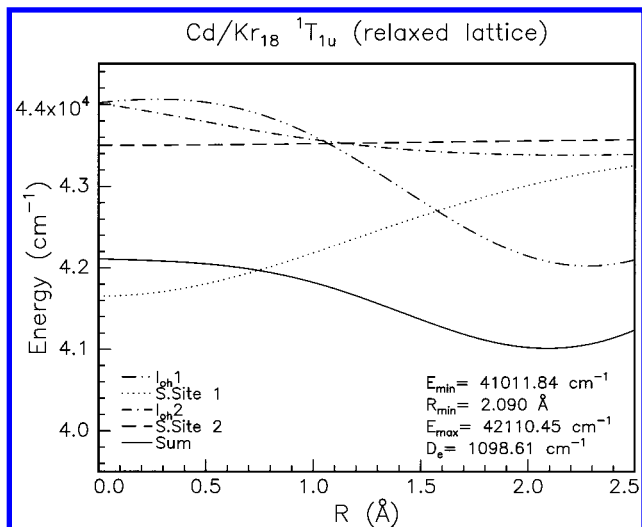


Figure 10. As in Figure 9 but for the movement of the “end” Kr atom into the next unit cell as the Cd(p_z) atom gets closer to the octahedral interstitial site. This alleviates the stress within the Cd/Kr system as the Cd(p_z) “end” Kr atom repulsive interaction is lessened. The destabilization caused by the Kr atom entering the next unit cell is counteracted by the stabilization of the Cd atom getting closer to the octahedral interstitial site. When these forces are equal, the “body mode” energy minimum is achieved.

in this figure. It is evident from the calculations that as the Cd atom moves from the substitutional site it occupies in the ${}^1A_{1g}$ ground electronic state toward the octahedral interstitial site, no stabilization arises in the Cd/Ne and Cd/Ar systems. In contrast, the Cd/Kr system, described in detail earlier, and the Cd/Xe system show excited-state stabilization in the body mode motion.

Absorption and emission energies can now be calculated assuming that vertical Franck–Condon transitions take place between the ground and excited electronic states. The formulas for calculating both of these energies are the following:

$$E_{\text{em}}(\text{cm}^{-1}) = E'(R'_{\text{min}}) - E''(R'_{\text{min}}) - E_{\text{Rg}\cdot\text{Rg}}$$

$$E_{\text{abs}}(\text{cm}^{-1}) = E'(R=0) - E''(R=0) \quad (9)$$

where $E_{\text{Rg}\cdot\text{Rg}}$ is the distortion energy in the rare gas lattice as the end rare gas atom is moved into its adjacent cell.

The predicted and recorded absorption energies are listed in Table 4. For the body mode of the Cd/Kr and Cd/Xe systems, there is relatively good agreement between the predicted and experimental results, but for Cd/Ar and especially Cd/Ne the agreement is poor. The calculated emission energies do not compare favorably with the recorded values, as seen in Table 5. The reason for the large discrepancy in the Cd/Kr system is thought to be due to the Cd•Kr ground-state potential curve being too repulsive. This problem arises because of the large extrapolation of the Cd•RG ground-state potential required to obtain energies at the short Cd•Kr bond length (~ 2.8 Å) existing at the stabilization displacement values (R'_{min}) in the excited state.

(ii) *Waist Mode.* The waist mode calculation is more straightforward than the body mode because it only involves a single variable, the in-phase contraction of four rare gas atoms (S.site1) toward the Cd atom. An overview of the interactions involved is shown in Figure 12. The contraction of the four rare gas atoms involves a single variable R_2 . There is also a fixed contribution from the two square-pyramid interactions belonging to $I_{\text{oh}1}$ and $I_{\text{oh}2}$ situated at fixed distances R_1 and R_3

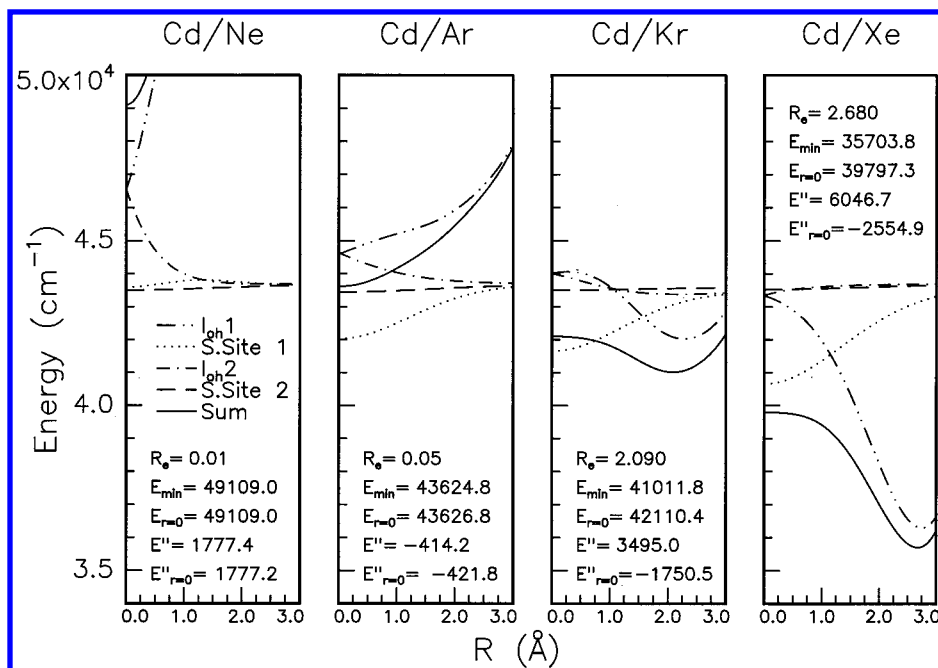


Figure 11. Body mode potential energy calculations for all the analyzed Cd/RG systems. Stabilization occurs for only Cd/Kr and Cd/Xe during this vibronic motion. Ground-state parameters are denoted by the “double prime” feature, although the potential energy curves from which they are calculated are not shown here. E_{\min} denotes the energy value at which the stabilization and destabilization forces (mentioned in the Figure 9 caption) are equal. All distances are in Å units, energy in cm^{-1} .

TABLE 4: Predicted Cd/RG $^1P_1 \leftarrow ^1S_0$ Absorption Wavelengths Obtained with Substitutional Site Occupancy^a

	$E'(r=0)^b$	$E''(r=0)^b$	λ_{abs} (nm)	λ_{obs} (nm)
Cd/Ne	49131.2	1774.6	211.16	220.2
Cd/Ar	43670.0	-421.8	226.80	221.0
Cd/Kr	42103.4	-1434.2	229.69	226.8
Cd/Xe	39804.6	-2536.1	236.18	235.6

^a The observed absorption wavelengths are shown for comparison

^b Energy units used are wavenumbers, cm^{-1} .

TABLE 5: Predicted $^1P_1 \rightarrow ^1S_0$ Emission Wavelengths in Nanometers for Body and Waist Modes of the Cd/Ar and Cd/Kr Systems^a

	observed	waist mode	body mode
Cd/Ar	233.5	241.5	
Cd/Kr	241.5, 262.0	273.2	315.3

^a The observed experimental emission is also shown for comparison, no body mode emission was observed for Cd/Ar.

with fixed angles θ_1 and θ_3 from the Cd atom. Another contribution to be included is the interaction between the Cd atom and the four next-nearest neighbors (S.site2), which depends on the fixed variables R_4 and θ_4 . The lattice changes produced by this waist mode motion can be viewed in Figure 13, which shows a “side on” view of the lattice XY plane. As the four nearest rare gas atoms from S.site1 contract, one can see these rare gas atoms detach themselves from the rare gas atoms they were bonded to on the diagonal, but in the process, they form four new rare gas–rare gas bonds with each other in a square plane.¹⁶ Thus, only a small destabilization of the lattice results from the waist mode as the breaking and forming of four rare gas bonds cancel each other. Figure 14 depicts the $^1T_{1u}$ electronic energy curves for the Cd/RG systems and lists important waist mode values, for both the ground and excited states.

Cd/Ne shows no stabilization for the waist mode calculation, a result also found in the body mode calculation. For Cd/Ar, Cd/Kr, and Cd/Xe excited-state stabilization occurs, the contrac-

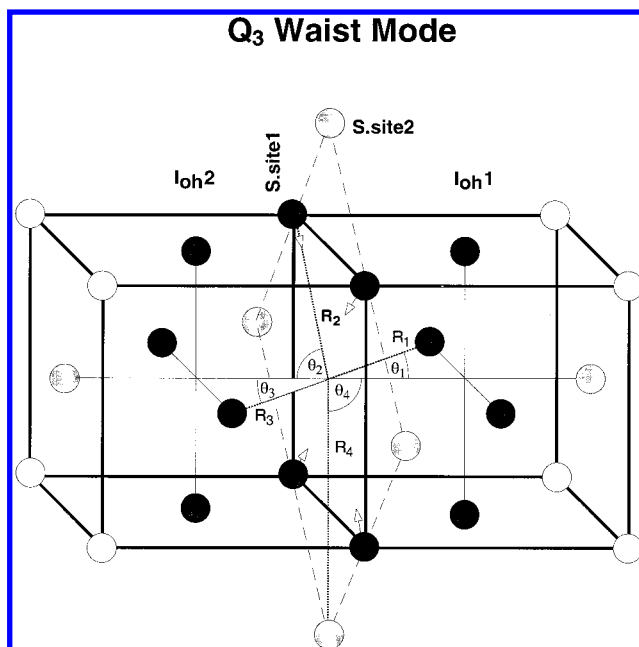


Figure 12. Angles and distance parameters utilized in the calculation of the “waist mode” (Q_3) motion. The four Kr atoms from S.site1 contract in-phase toward the Cd atom in the XY plane. Waist mode calculations also involve the fixed contributions: $I_{\text{oh}1} + I_{\text{oh}2}$ and that from S.site2.

tions of the respective rare gases (S.site1) are 0.47, 0.82, and 1.07 Å as listed in Figure 14. The stabilization energy also increases as the rare gas atom size gets bigger. The calculated singlet absorption wavelengths are given in Table 4. These values are identical to those derived from body mode because they are both calculated at $R = 0$, corresponding to zero displacement from the substitutional site.

Discussion

Table 6 shows a comparison between the number of observed and predicted $^1P_1 \rightarrow ^1S_0$ emission bands for the four Cd/RG

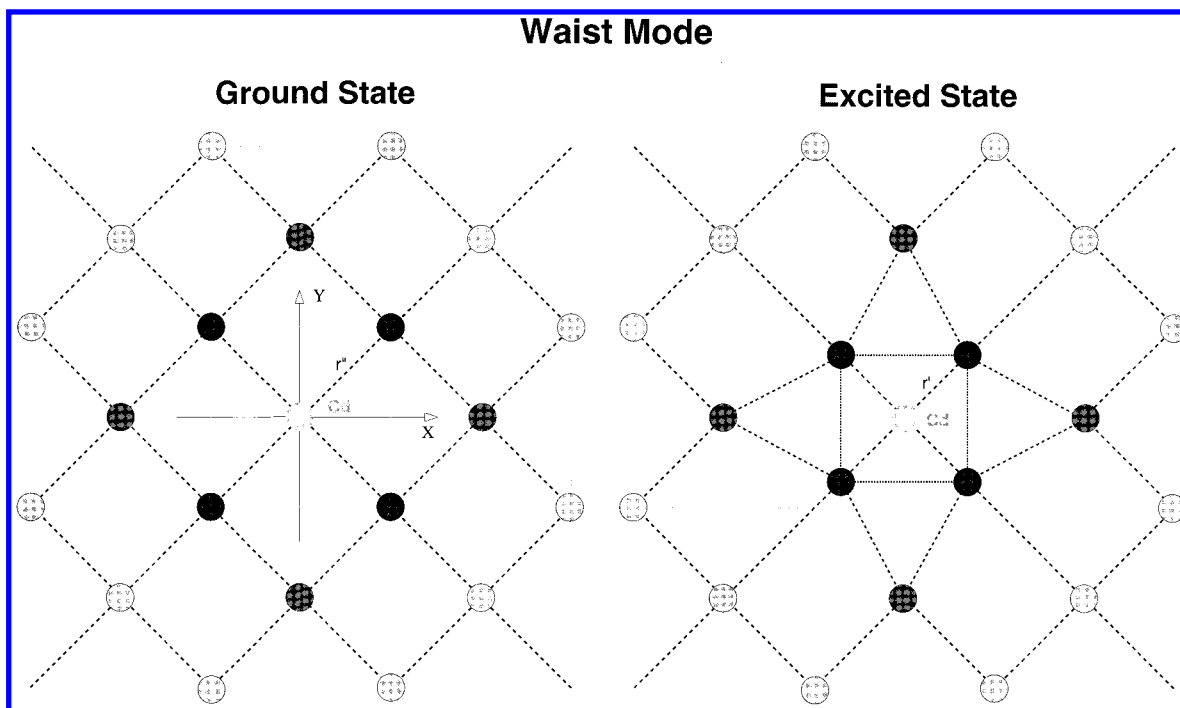


Figure 13. "Side-on" view through the adjoining unit cells of both the ground and excited states involved with the "waist mode". In the excited state, the four Kr atoms contract in the XY plane toward the Cd atom, detaching themselves from four Kr atoms but also forming four new Kr–Kr bonds in the process. These forces balance each other, but as the atoms contract, eight Kr–Kr bonds are distorted. Thus, there is a small net destabilization of the lattice.

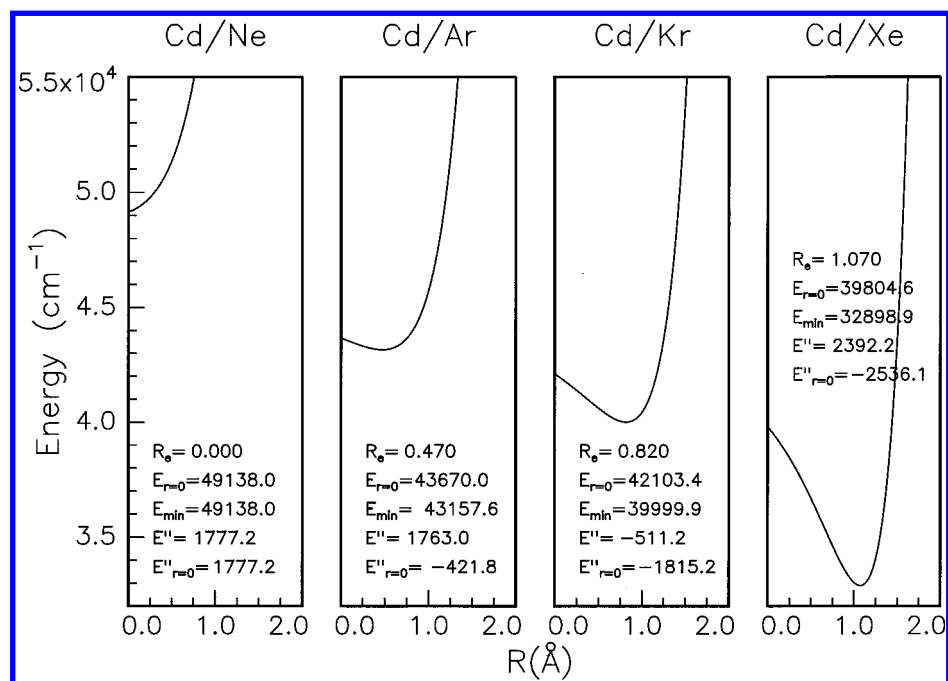


Figure 14. Potential energy plots for the vibronic "waist mode" in the Cd/RG systems. Stabilization occurs for Cd/Ar, Cd/Kr, and Cd/Xe. As with the "body mode" plots, important ground-state parameters are listed. At R_{min} , the destabilization of the lattice is equal to the stabilization induced by the in-phase contraction of the four Kr atoms toward the Cd atom. All distances are in Å units, energy in cm^{-1} units.

solids. Predictions for both Cd/Ar and Cd/Kr compare favorably with observation. In the Cd/Kr system, two singlet emission bands are predicted in line with observation. The body and waist mode motions exist in this system and lead to distinct excited-state energy minima from which two spectrally resolved emission bands occur. In all the Cd/RG systems, with the exception of Cd/Ne, the waist mode leads to a lowering of energy. The existence of stabilization on the body mode in Cd/Kr, corresponding to motion of the Cd atom from the substitutional site toward an adjacent octahedral interstitial site, is

TABLE 6: Comparison of the Number of Singlet Emission Bands Predicted with Those Observed for the Cd/RG Matrix Systems

	observed	predicted
Cd/Ne	one	none
Cd/Ar	one	one
Cd/Kr	two	two
Cd/Xe	none ^a	"two"

^a Singlet emission is not observed in this system because of very efficient intersystem crossing.

due to the favorable size matching between the bond length of the diatomic Cd•Kr $C^1\Pi_1$ excited state (3.17 Å) and the distance of the Kr atoms to the center of the octahedral interstitial site (2.82 Å). In Cd/Ar the bond length of the $C^1\Pi_1$ state is 1.655 Å larger than the octahedral interstitial site, so repulsive interactions immediately set in, precluding stabilization of the body mode in the Ar lattice. This behavior is consistent with the single emission band recorded in the Cd/Ar matrix system. Cd/Ar shows stabilization only for the waist mode calculation, so this vibronic mode is identified as producing the recorded luminescence. The assumption inherent in the simulations, that a Cd atom will occupy a single substitutional site in Ar and Kr lattices, is thus plausible.

Correct prediction of the spectral position of the singlet emission energies has proved difficult for the Cd/Kr system, as can be seen in Table 5. However, the trend exhibited in the excited-state stabilization energies, as illustrated in Figures 11 and 14 for the body and waist mode $^1T_{1u}$ excited-state curves, is similar to those pertaining to the Zn/RG matrix systems. The absorption wavelength calculated for Cd/Ar showed a difference of 5.8 nm compared with its observed equivalent. The predicted values were obtained assuming the Cd atom occupies an undistorted substitutional site in the ground $X^1\Sigma_0$ state. By viewing Table 6, we can see that the substitutional site diameter of the Ar solid is 3.756 Å whereas the Cd•Ar ground-state bond length is 4.31 Å, so the Cd atom is relatively cramped in a substitutional site of Ar. Given the 3-fold splitting clearly observed on the Cd/Ar absorption band,⁴ which indicates Jahn–Teller coupling is occurring, it is likely that the Cd atom is residing in a highly symmetrical site in the ground state such as a substitutional site.¹⁷

Further calculations were done to identify the extent of expansion of the substitutional site of Ar with ground-state atomic cadmium occupancy. These involved equalization of the stabilization energy associated with allowing the 12 nearest-neighbor Ar atoms to expand away from the Cd atom and the destabilization the motion of these argon atoms¹⁸ has on the lattice. The energies were obtained using eq 1 and the ground-state Cd•Ar and Ar₂ potentials listed in Table 1. Calculation showed an expansion of 0.196 Å in the substitutional site diameter with a resulting stabilization of 374.2 cm⁻¹. When the excited-state calculations were rerun with the lattice parameter increased by 0.277 Å (0.196 × √2), an absorption wavelength of 225.3 nm was obtained, which compares better with the observed value at 222.2 nm than the 226.8 nm value obtained with the cramped substitutional site.

In Cd/Ne, a singlet emission band is not predicted even though a band is observed. The agreement between the predicted and observed wavelengths is poor in this system. As in the Cd/Ar system, the assumption of substitutional site occupancy of Cd in Ne is the most likely reason for the discrepancy. The Cd atom will be severely cramped in a substitutional site of Ne, which has a diameter of only 3.154 Å compared to the bond length of Cd•Ne in the ground state, which is 4.26 Å. The absence of the 3-fold splitting in the excitation profile of Cd/Ne in Figure 1 and the poor comparisons between observed and predicted results suggest that the Cd atom does not occupy a substitutional site in the ground state but a multivacancy site.

Further calculations were performed to examine whether a tetravacancy is the site atomic Cd occupies in a neon matrix. These involved obtaining the extent of destabilization on the lattice by allowing the very cramped substitutional site of Ne to expand when occupied by a Cd atom. An increase of 0.324 Å in the substitutional site diameter was obtained in exactly

the same manner as outlined above for Cd/Ar. The resulting lattice destabilization was found to be 402.8 cm⁻¹. The energy of tetravacancy site occupancy was obtained by balancing the stabilization arising from the contraction of the 24 nearest-neighbor Ne atoms surrounding the Cd atom and the 72 Ne–Ne interactions changed with the Cd–Ne contraction. The lattice destabilization energy was 233 cm⁻¹, significantly less than the 402.8 cm⁻¹ accompanying the expanded substitutional site occupancy, indicating the site occupancy to be tetravacancy.

Inspection of the body and waist mode plots for Cd/Xe (Figures 11 and 14) shows that stabilization occurs for both modes in this system. Hence, two singlet emission features are predicted. This is not the case though because two triplet emission features are observed experimentally.⁴ The reason for the absence of singlet emission is attributed to intersystem crossing (ISC) from the excited singlet state $^1T_{1u}$ to the metastable triplet $^3T_{1u}$ state. This behavior is also exhibited in the diatomic Cd•Xe van der Waals complex.¹⁹ The mechanism proposed by Breckenridge for ISC in diatomic Cd•Xe is a crossing of the bound $^1\Pi_1$ potential curve by the repulsive $^3\Sigma^+$ state curve, leading to predissociation of the former state and production of triplet-state atomic cadmium. Excellent agreement exists between the observed and predicted Cd/Xe absorption wavelengths, even though Cd•Xe possesses the strongest interactions of the Cd•RG systems. Table 3 shows that the larger the rare gas atom, the better the match between the substitutional site diameter and the Cd•RG $X^1\Sigma_0$ bond length. Thus, of all the solid rare gases, atomic Cd fits most easily in the substitutional site of Xe.

Conclusions

Simulations carried out on the singlet luminescence of the Cd/RG systems can be deemed a qualitative success because comparisons with observed and predicted singlet emission features worked well for Cd/Ar and Cd/Kr. Predicted emission wavelengths though are not comparable to those observed possibly because of the highly repulsive nature, especially for Cd/Kr, of the $^1A_{1g}$ ground state. A reasonable argument is given for the discrepancy between the observed and predicted Cd/Ne data. More work needs to be performed on the Cd/Ne system, since spectral simulations must be carried out on Cd occupying the tetravacancy site predicted above as the more stable site.

The key conclusions to be gleaned from these calculations are the following. (1) Cd occupancy is in single substitutional sites of Ar, Kr, and Xe hosts with little or no distortion in the Xe lattice and considerable expansion of the surrounding spheres in Ar. Calculations based on single substitutional site occupancy of Cd in Ne are not consistent with observations. In neon a multivacancy site occupancy is expected from spectral observations and site occupancy calculations.

Singlet emission gives qualitative agreement between experiment and theory. In Cd/Ar, where a single emission band is observed, only the waist mode leads to excited-state stabilization. In Cd/Kr, which exhibits a pair of singlet emission bands, both waist and body modes lead to energy minima. The Cd/Ar behavior contrasts with the Zn/Ar (and Zn/Kr) for which pairs of minima were identified in line with observation. The difference between the Zn/Ar and Cd/Ar systems clearly originates from the larger size of the diatomic Cd•Ar $X^1\Sigma_1$ and $C^1\Pi_1$ states compared with the smaller values in diatomic Zn•Ar. The longer bond length in the ground state of Cd•Ar means atomic cadmium is cramped in a substitutional site of Ar. Indeed, experiments show⁴ that upon deposition, a pair of sites exist in the Cd/Ar matrix system, with removal of the thermally unstable “red” site never fully complete.

Acknowledgment. The experimental portion of this research was funded by the European Union, TMR 1996–1998, “Access to Large Scale Facilities” Program (Grant No. ERBFMGECT 950059) and the Irish Government *Forbairt* Basic Science Research Scheme. B.H. also gratefully acknowledges *Forbairt* for receipt of a Ph.D. studentship.

References and Notes

- (1) McCaffrey, J. G.; Ozin, G. A. *J. Chem. Phys.* **1994**, *101*, 10354.
- (2) Bracken, V. A.; Gürtler, P.; McCaffrey, J. G. *J. Chem. Phys.* **1997**, *107*, 5290.
- (3) Crepin, C.; Tramer, A. *J. Chem. Phys.* **1992**, *97*, 4772.
- (4) Healy, B.; McCaffrey, J. G. *J. Chem. Phys.* **1999**, *110*, 3903.
- (5) McCaffrey, J. G.; Kerins, P. N. *J. Chem. Phys.* **1997**, *106*, 7885.
- (6) McCaffrey, J. G.; Healy, B. Unpublished results of 1999.
- (7) Zuniga, J.; Bastida, A.; Requena, A.; Halberstadt, N.; Beswick, J. A. *J. Chem. Phys.* **1993**, *98*, 1007.
- (8) Bastida, A.; Zuniga, J.; Requena, A.; Soep, B.; Halberstadt, N.; Beswick, J. *J. Chim. Phys. (Paris)* **1995**, *92*, 384.
- (9) Kerins, P.; McCaffrey, J. G. *J. Chem. Phys.* **1998**, *109*, 3131.
- (10) Funk, D. J.; Kvaran, A.; Breckenridge, W. H. *J. Chem. Phys.* **1989**, *90*, 2915.
- (11) Funk, D. J.; Breckenridge, W. H. *J. Chem. Phys.* **1989**, *90*, 2927.
- (12) The $A e^{-bR}$ gives the potential energy curve a repulsive nature, where the C_6/R^6 provides an attractive portion to this curve.
- (13) Kaup, J. G.; Breckenridge, W. H. *J. Phys. Chem.* **1995**, *99*, 13701.
- (14) Roncero, O.; Beswick, J.; Halberstadt, N.; Soep, B. *Dynamics of Polyatomic van der Waals Complexes*; Halberstadt, N., Janda, K., Eds.; Plenum Press: New York, 1990; p 471.
- (15) Absorption to the 1A_1 state of the CdKr₄ cluster is predicted at 225.33 nm, and emission from this state is predicted at 399.83 nm. Hence, the absorption transition will be slightly to the blue of the atomic transition while a large red shift is expected in the emission.
- (16) The “new bond formation” resulting from the excited-state waist mode is depicted in Figure 13. Thus, four new bonds are formed by the approaching four rare gas atoms when they have created the central square shown on the right of Figure 13, while four bonds on the axis of motion (the four diagonals) have been weakened. Examination of Figure 13 reveals that in the ground state the four atoms undergoing motion in the waist mode are not in direct contact; i.e., they are not at the equilibrium bond length of the rare gas dimer. They are in fact positioned at a distance of the lattice parameter, with a vacant octahedral interstitial site located between them. The extent of bond formation and bond breakage is nearly equal and just about cancels each other out in the waist mode. However, a much more minor extension of eight RG–RG interactions from equilibrium will always result in a energy increase, albeit small. The eight RG–RG interactions in question are the eight bonds connecting the contracting rare gas atoms (S.site1) and those from the next-nearest neighbors (S.site2) have been distorted, as depicted in the right panel of Figure 13, and are thus weakened.
- (17) Hoffmann-Millack, B.; Klein, A.; Lagier, H.; Maid, B.; Hormes, J. *J. Chem. Phys.* **1989**, *136*, 453.
- (18) Outward motion of the 12 argon atoms surrounding the guest cadmium atom in a substitutional site results in a compression of the 12 Ar–Ar distances directly on-axis and an expansion of the 24 Ar–Ar interactions existing on the surface of the first-sphere atoms. Because all the atoms undergoing motion are next-nearest neighbours, the Ar–Ar expansions and contractions mentioned will be identical in magnitude with the extent of the Cd–Ar expansion. The total number of Ar–Ar interactions changing as a result of the substitutional site expansion is thereby 36.
- (19) Bililign, S.; Gutowski, M.; Simons, J.; Breckenridge, W. H. *J. Chem. Phys.* **1993**, *99*, 3815.